ELSEVIER

PII: S1359-8368(96)00067-4

Composites Part B **28B** (1997) 453–464

1359-8368/97/$17.00

Finite element simulations of textile composite forming including the biaxial fabric behaviour

P. Boisse[a,b,*], M. Borr[c], K. Buet[b] and A. Cherouat[a]

[a]*Laboratoire de Modélisation et Mécanique des Structures, Université Paris 6, ENSAM, ENS Cachan, Paris, France*

[b]*Ecole Supérieure de l'Energie et des Matériaux, Orléans, France*

[c]*Laboratoire de Mécanique Appliquée, Université de Franche Comté, Besançon, France*

(Received 23 July 1996)

A finite element simulation of fibre fabric shaping process is proposed. The behaviour of fabrics is experimentally studied from biaxial tensile tests on cross shaped specimens. These experiments permit to investigate the influence on the fabric behaviour of the undulation variations of the weaving and of the interactions between warp and weft yarns. A constitutive model including these aspects is proposed, validated and identified from the biaxial tests. Finite elements made of woven yarns are built in the field of non-linear kinematics. The deformation energy is calculated as the sum of the energy of each elementary cell for which the biaxial behaviour previously identified is considered. A drawing simulation with square punch and die is presented. It allows to distinguish the geometries of the tools which are possible or not for the shaping process. The influence of the undulation variations are studied in a second example. © 1997 Elsevier Science Limited.

(Keywords: fabric behaviour; biaxial test; finite elements; shaping simulations)

NOTATION

$\alpha, \beta, \gamma, \delta$	Indexes equal to 1 or 2
$\boldsymbol{x}_1, \boldsymbol{x}_2$	Mean plane vectors of the fabric.
$\boldsymbol{x}_3$	Normal vector of the fabric
L_{0_α}	Inter-yarn length.
e_{0_α}	Distance between mean axis of yarn α and mean plane of the fabric.
θ_α	Angle between yarn α and axis $\boldsymbol{x}_3$.
w_α	Displacement of point $\mathbf{P}_\alpha$ along $\boldsymbol{x}_3$.
ε_{f_α}	Strain of yarn α.
T_f^α	Tension of yarn α.
F_c	Compression force between the two yarns along $\boldsymbol{x}_3$.
$\boldsymbol{u}$	Displacement vector of a point M at an initial position $\boldsymbol{x}_0$.
N^k	2D interpolation function related to node k.
$D_u(\boldsymbol{A})\boldsymbol{\delta} = \frac{\mathrm{d}}{\mathrm{d}\lambda}(\boldsymbol{A}(\boldsymbol{u}+\lambda\boldsymbol{\delta}))_{\delta=0}$	Fréchet derivative of **A** with regard to $\boldsymbol{u}$ in the direction $\boldsymbol{\delta}$.
$\boldsymbol{\eta}$	Virtual displacement field.
$\boldsymbol{S} = S^{\alpha\beta}\boldsymbol{h}_{\alpha 0} \otimes \boldsymbol{h}_{\beta 0}$	Second Piola–Kirchhoff stress tensor.
$\boldsymbol{T} = T^{\alpha\beta}\boldsymbol{h}_{\alpha 0} \otimes \boldsymbol{h}_{\beta 0}$	Lagrangian tensile tensor.
$\boldsymbol{E} = E_{\alpha\beta}\boldsymbol{h}^{\alpha 0} \otimes \boldsymbol{h}^{\beta 0} = \bar{E}_{\alpha\beta}\boldsymbol{g}^{\alpha 0} \otimes \boldsymbol{g}^{\beta 0}$	Green–Lagrange strain tensor.
$\boldsymbol{W} = T^{\alpha\alpha}L_{0_\alpha}\boldsymbol{h}_{\alpha 0} \otimes \boldsymbol{h}_{\alpha 0} = \bar{W}^{\alpha\beta}\boldsymbol{g}_{\alpha 0} \otimes \boldsymbol{g}_{\beta 0}$	Lagrangian static tensor.
$\boldsymbol{D} = \frac{\partial \boldsymbol{W}}{\partial \boldsymbol{E}} = \bar{D}^{\alpha\beta\gamma\delta}\boldsymbol{g}_{\alpha 0} \otimes \boldsymbol{g}_{\beta 0} \otimes \boldsymbol{g}_{\gamma 0} \otimes \boldsymbol{g}_{\delta 0}$	Behaviour tensor of the fourth order.
$\|\boldsymbol{u}\|$	Norm of vector $\boldsymbol{u}$.
$\boldsymbol{h}_{10}, \boldsymbol{h}_{20}$	Initial unit vectors, in the yarn directions.
$\boldsymbol{h}^{10}, \boldsymbol{h}^{20}$	Contravariant vectors associated to $\boldsymbol{h}_{10}, \boldsymbol{h}_{20}$.
$\boldsymbol{g}_{10}, \boldsymbol{g}_{20}, \boldsymbol{g}_1, \boldsymbol{g}_2$	Initial and current material vectors in the mean plane of the fabric.
$\boldsymbol{g}^{10}, \boldsymbol{g}^{20}$	Contravariant vectors associated to $\boldsymbol{g}_{10}, \boldsymbol{g}_{20}$.
$\boldsymbol{B}$ with $D_u(\bar{E}_{\alpha\beta})\boldsymbol{\eta} = \bar{B}_{\alpha\beta s}\eta_s$	Strain interpolation matrix.
$\boldsymbol{K}^e$	Elementary stiffness matrix.
$\boldsymbol{K}_\sigma^e$	Elementary geometrical stiffness matrix.
$\boldsymbol{F}_{\text{int}}^e$	Elementary internal load vector.

*Correspondence to: Prof P. Boisse, Laboratoire de Modélisation et Mécanique des Structures, Université Paris 6, Tour 66, 5ème Etage, Boite 161, 4 place Jussieu, 75252 PARIS Cedex 05, FRANCE, Tel: (33) (1) 44 27 41 60, Fax: (33)(1) 44 27 71 60, e-mail: pboisse@univ-orleans.fr

INTRODUCTION

Fibre fabrics (glass, carbon, kevlar...) are very efficient reinforcements for thin composite materials. The manufacturing of textile composite structures with complex shapes can be obtained by deep drawing of an initially flat fibre fabric, prior to the resin injection (R.T.M. process)[1,2] or prior to resin hardening.[3] For a given fabric and a given 3D surface, a main question is whether the shaping operation is

possible. Efficient computational programs have been developed in the last few years for the simulation of metal sheet forming especially in automotive industries.[4–6] The metal blank is submitted to large membrane strains and consequently to significant thickness variations. Thickness distribution and its consequences (such as the possible tearing of the metal sheet) are one of the main results of the computation. The deformation of a fabric during a shaping process is very different. The strains in the directions of the yarns are small ($\leq 2\%$ for glass fibre yarns as shown later). The deformation of the fabric into a non developable surface is mainly due to angular variations between the warp and weft yarns.

The purpose of the present paper is to describe a simulation tool of the fabric shaping process. Computational simulations of such problems have been proposed, mainly based on geometrical approaches.[7,8] The present work is based on a mechanical approach and a finite element method. It defines the deformation state in the fabric during the forming process on the one hand, and the tension state of the fibres on the other hand. These two quantities are important and must be checked to define whether the deep drawing is possible. In particular, in-plane shear deformations are the main phenomenon of the fabric deformation. They are significant (up to 60° in some cases) but a limit value exists above which yarns are overlapping, and this leads to local folding. Tensions in the yarns also have to remain lower than the fracture value of each yarn.

In a first section, the mechanical behaviour of fabrics is analysed from biaxial tests. These ones allow to point out the non-linearities induced by undulation variations of the yarns during the deformation. The phenomenon is biaxial considering that warp and weft yarns are linked because of the weaving. As a consequence, the experimental study is carried out by the mean of a biaxial tensile device on cross-shaped specimen. A model for the behaviour, based on local equilibrium of the elementary pattern, is identified. It properly expresses the phenomenon of the progressive hardening that appears at the beginning of the tensile test and which is linked to undulation variations of the yarns.

In a second section, a finite element simulation is presented. Elements made of woven yarns are built in the field of large strains. The deformation energy is calculated as the sum of the energies of each elementary cell which includes the behaviour previously defined.

MECHANICAL BEHAVIOUR OF FIBRE FABRICS

Studies relative to textile structural composites behaviour, i.e. matrix reinforced by woven fabrics, are very numerous. The problem mainly consists in defining the characteristics of an equivalent homogeneous material and forecasting the matrix damage under high load.[9–11] For the woven fabric alone, the problem is quite different because the absence of resin allows relative yarn displacements which mainly influence the global fabric behaviour.

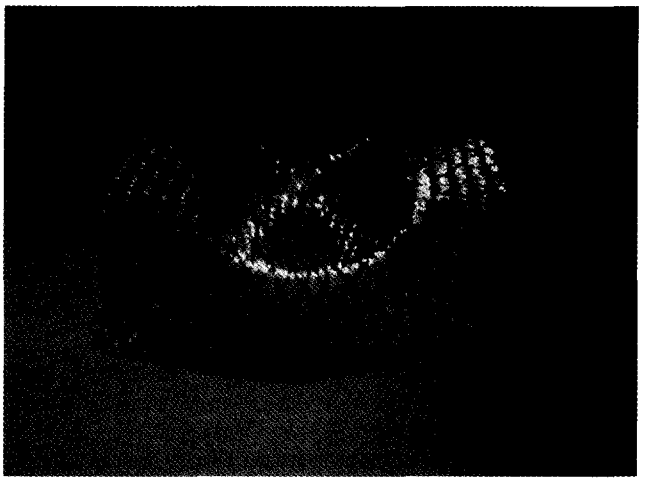

Figure 1 Deformation of the fabric. Straight lines have been drawn in the weft and warp directions prior to forming

Absence of shear stiffness

The first consequence for a classic woven fabric with two fibre directions is the absence of the in-plane shear stiffness due to angular variations between warp and weft yarn directions (a phenomenon sometimes called trellising). These variations are significant (up to 60° in some cases) (*Figure 1*). Consequently, the modelling used for the fabric behaviour will have to account for large displacements but also for large strains.

Absence of bending stiffness

Yarns consist of very small section fibrins whose bending stiffness is negligible, therefore these of yarns and fabric are negligible too. The yarn or fibrin buckling being immediate under a compression load, the fabric compressive stiffness can also be neglected.

Absence of interfibre sliding between warp and weft directions

The evolution of a straight line grille drawn on the fabric prior to shaping, shows that the fabric can be considered as a continuous 3D surface domain (*Figure 1*). Actually, the drawn lines become curved but remain continuous. Taking into account that these lines have been drawn alternatively on warp and weft yarns, it can be deduced that there is no interfibre sliding (in any case, far enough from the fabric edges) and that two initially superimposed yarns remain superimposed during the deformation process. This non-sliding condition is ensured by the weaving and the friction between yarns. One of the main consequences is the possibility to use a classic Lagrangian finite element approach for the surface domain of the fabric, as done in section "Finite element simulation".

Influence of undulation variations. Geometric non-linearities on a mesoscopic scale

A characteristic aspect of woven fabrics is connected with

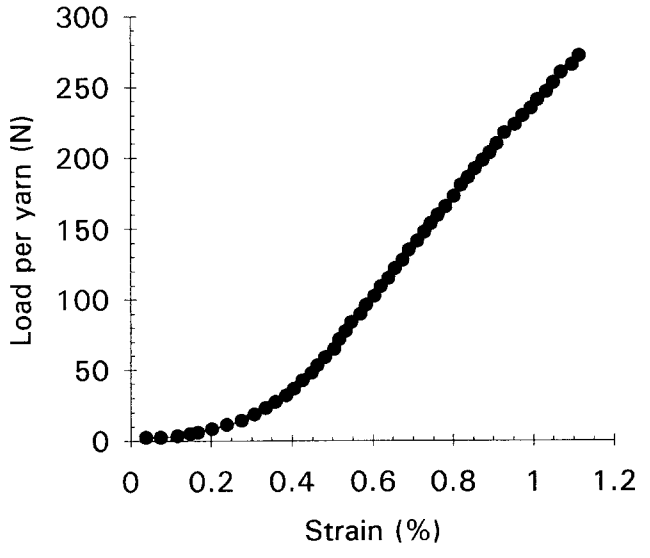

Figure 2 Tensile test in the yarn direction

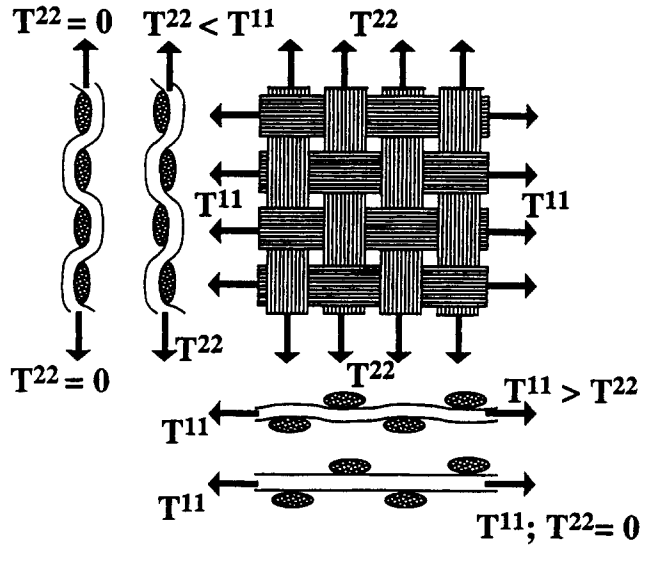

Figure 3 Undulations and interactions

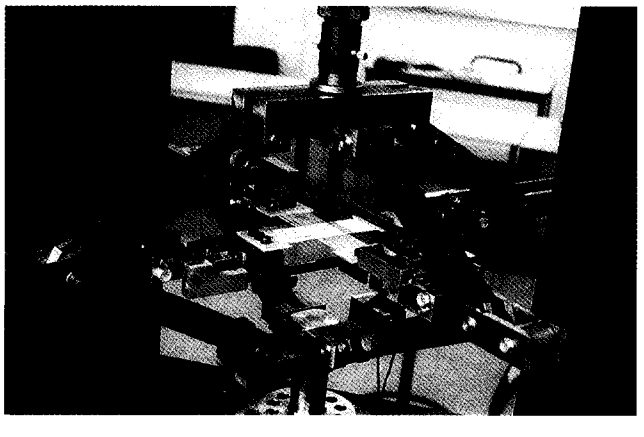

Figure 4 Biaxial tensile device

the absence of resin and is the influence of undulation variations while the fabric is being loaded. A uniaxial test in the yarn direction classically shows a progressive hardening area before a linear zone (*Figure 2* for a glass fibre plain-weave fabric).

In many cases, this non-linear area concerns large strain values compared to the one of the entire woven structure (strains before fracture in the yarn direction remain low, about 2% for glass fibres). Accordingly, this aspect has to be taken into account in the modelling of the material mechanical behaviour.

In fact, the fabric global tensile behaviour results from yarn deformation, on the one hand, and from the tendency the yarn has to straighten, on the other hand (*Figure 3*).

The previous phenomenon is part of the geometric non-linearities on the mesh scale. It is not strictly microscopic because undulations due to weaving are quite large (a few millimetres). Nevertheless, this scale is smaller than the one of the fabric structure under consideration, so we will speak of mesoscopic phenomenon. Moreover, it is a biaxial problem because of the woven character of the structure. When the undulation decreases in one direction, it tends to increase in the other direction. So the behaviour modelling will have to be biaxial and to relate both warp and weft strains to both warp and weft tensions.

The translation of undulation modifications, on the mesh scale, into a global non-linear behaviour is a particular case of the non-linear mechanics of materials where the material-type non-linearities, on a macroscopic scale, translate some geometric-type or contact-friction-type non-linearities, on a microscopic scale. Friction plays a significant role in fabric mechanical behaviour. It ensures material continuity (of 3D surface-type) by imposing to two initially superimposed yarns to remain superimposed during the deformation (see section "Absence of interfibre sliding"). It can also be noted that the tensile load-strain curves are reversible, at least for a large range of woven materials like these presented in the following paper. So, there is no (or little) energy dissipation due to friction. Friction will only be implicitly taken into account in the proposed modelling by giving a meaning to the notion of warp and weft strains, in a woven continuous medium, linked to warp and weft tensions by a non-linear elastic law.

Biaxial test

Considering the previous remarks, the experimental study, used to determine the fabric behaviour, is based on a biaxial tensile device. It aims at obtaining, for a given fabric, experimental results expressing undulation and interaction phenomena and allowing to validate and identify (see section "Identification of a biaxial model") a representative model for fabric behaviour. The choice of cross shaped specimen for biaxial tensile tests is well suited to fabric problem. The main objection encountered with this kind of tests when they are performed on classic rigid materials (metal for example) lies in stress field inhomogeneity inside the specimen, notably near its inner corners.

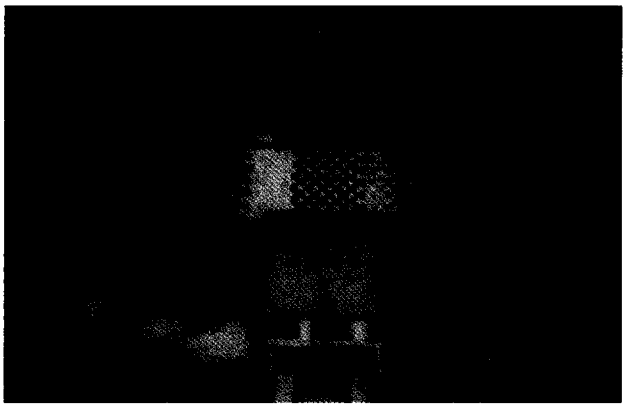

Figure 5 Cross shaped specimen. Definition of initial state

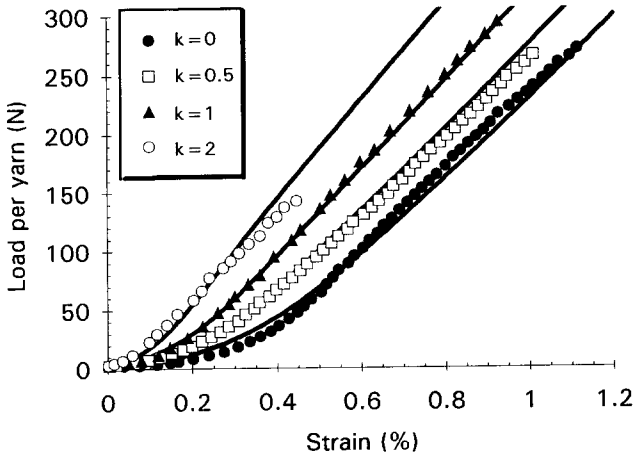

Figure 6 Biaxial tensile test of glass fibre plain-weave fabric. Experimental results and modelling (in solid line) for various ratios k = strain in warp direction/strain in weft direction

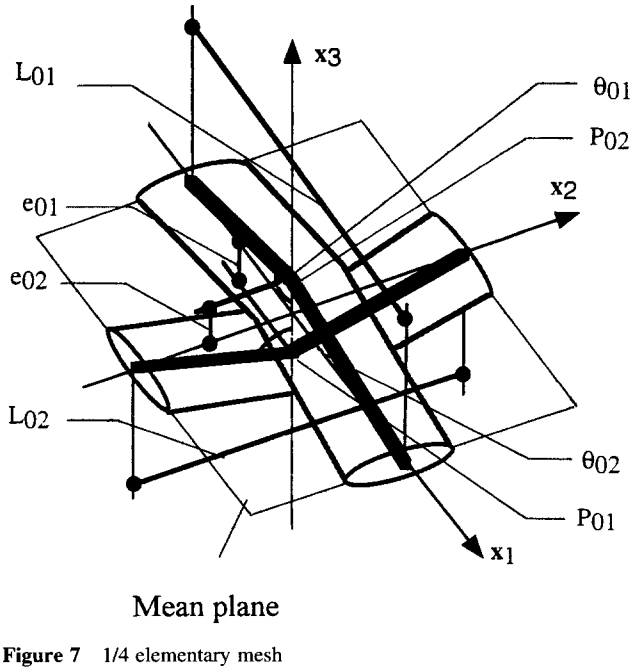

Figure 7 1/4 elementary mesh

The fabric having no shear stiffness, this problem is avoided. The device used (*Figure 4*) imposes homogeneous strain field, in variable ratios between warp and weft directions. This device is based on the kinematics of a double four-bar device which has been proposed for metallic materials.[12] This kind of kinematics ensures, in a simple way, the fixity of the specimen symmetry axes during the test. To ensure an efficient maintenance of the specimen in the jaws, the cross ends are stiffened by prepregs.

Classic means to measure strains cannot be used on active area of the specimen. In particular, fibrous texture precludes the using of strain gages. Furthermore, the relative displacement of the jaws is not directly significant considering the non-woven part of the cross shaped specimen. An optical measurement of the strain, by photographing on very fine grain film and using a great enlargement, proved very efficient. Getting yarn displacements is easy and using a scanner to digitize it, and then, a picture processing software, leads to a good accuracy (an about 0.5% error) on strain measurement.[13] A great advantage of this device lies in the simultaneous acquisition of the strain in each point. It also allows to check whether the deformation is homogeneous on the entire woven area. This checking is determining and enables an optimization of certain parts of the device. Moreover, experimental procedures can be validated.

In fact, defining the initial configuration of the specimen is an essential step in fabric tests. Woven structure has no shear or compressive stiffness, and its tensile stiffness is very low when stress is zero, as a consequence, initial state is not strictly defined. This leads, if no specific measure is adopted, to erroneous results pointed out because they can not be repeated. To overcome this difficulty, the initial dimensions of the specimen are defined under a low tensile effort (a few deciNewton per yarn) imposed by the device presented in *Figure 5*. A boring device enables to calculate the specimen right dimensions in this position. So, initial state is clearly defined and tests are well repeated. *Figure 6* represents test results for different strain ratios in the case of a glass fibre plain-weave fabric. A progressive hardening area, linked to undulation decreasing and coming before a zone of linear behaviour, is clearly noticed. When the two strains are not equal, undulation decreasing, and so, progressive hardening, are more significant in the direction of the higher strain. The phenomenon is very more limited, even nil, in the other direction. These different points are schematized on *Figure 3*.

Identification of a biaxial model

Experimental data, previously obtained, allow the identification of a biaxial model for fabrics. Several approaches are possible.[14,15] The model presented here for plain-weave fabrics is part of models based on the equilibrium of an elementary mesh during its deformation.[16,17] The model links both warp and weft tensions $T^{\alpha\alpha}$ (α = 1 or 2) to both warp and weft strains $\epsilon_{\alpha\alpha}$. x_1, x_2 describe the mean plane of the fabric, and x_3 its normal. The

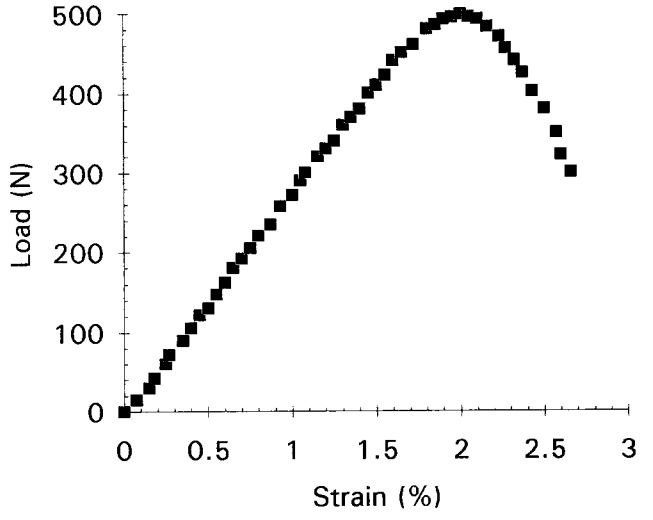

Figure 8 Tension *versus* strain curve for a single fibre yarn

initial geometric characteristics $L_{0_\alpha}, e_{0_\alpha}$ are defined on *Figure 7*. The following intermediate variables are used:

ε_{f_α}: strain of yarn α.

T_f^α: tension of yarn α.

θ_α: angle between yarn α and axis x_3.

w_α: displacement of point P_α along x_3.

F_c: compression force between the two yarns along x_3.

A tensile test on a yarn allows the identification of the tensile behaviour. Contrary to load-strain tensile curves for fabrics, the one of a yarn is straight until a progressive breaking of the threads (*Figure 8*). It will be assumed that this limit is not reached, and the simulation presented in section "Numerical examples" permits to check this state of tension. This is a great advantage of the mechanical approach in regard to geometrical approaches like 3D wrapping.[7,8]

The tensile behaviour of each yarn α (α = 1 or 2) (*Figure 8*) is expressed by

$$T_f^\alpha = C^\alpha \varepsilon_{f_\alpha} \tag{1}$$

and the behaviour in transverse compression is supposed to be:

$$w_1 - w_2 = A\left(1 - e^{-BF_c}\right) \tag{2}$$

The mesh geometry imposes:

$$\varepsilon_{f_\alpha} = \frac{\left(4\left(e_{0_\alpha} + \lambda_\alpha w_\alpha\right)^2 + L_{0_\alpha}^2\left(1+\varepsilon_\alpha\right)^2\right)^{1/2}}{\left(L_{0_\alpha}^2 + 4e_{0_\alpha}^2\right)^{1/2}} - 1 \tag{3}$$

where

$$\lambda_\alpha = -1 \text{ if } \alpha = 1$$

and

$$\lambda_\alpha = 1 \text{ if } \alpha = 2$$

$$\cos\theta_\alpha = \frac{2\left(e_{0_\alpha} + \lambda_\alpha w_\alpha\right)}{\left(L_{0_\alpha}^2\left(1+\varepsilon_\alpha\right)^2 + 4\left(e_{0_\alpha} + \lambda_\alpha w_\alpha\right)^2\right)^{1/2}} \tag{4}$$

Equilibrium of points P_α and of the entire mesh leads to:

$$T_f^1 \cos\theta_1 = T_f^2 \cos\theta_2 \quad T^{\alpha\alpha} = T_f^\alpha \sin\theta_\alpha \quad F_c = 2T_f^\alpha \cos\theta_\alpha \tag{5}$$

The system of equations (1)–(5) links tensions T^{11}, T^{22} to strains ϵ_{11}, ϵ_{22}. When the strains are given, the tensions can be found by solving a simple non-linear equation [obtained after several substitutions on eqn (5)] with w_α as the unknown. This quantity allows the determination of the others.

The experimental study presented in section "Biaxial test" makes possible the validation of the model described above and the identification of the necessary coefficients (*Figure 6*). In particular, it underlines the crucial role played by the behaviour of the yarn in transverse compression. In this direction, the yarns are quite stiffless so they are flattened a lot, when the loading is started. Undulation variations are found higher when considering the yarn compressible than when considering it incompressible. Some models are based on this last hypothesis[16] and the present experimental study shows that they can not express the really observed behaviour. For example, this flattening explains the non-linear area when warp and weft strains are equal. Because quantifying this transverse behaviour by experimental means is hard to perform, the coefficients that define eqn (2) are identified thanks to biaxial tensile curve when warp and weft strains are equal. Considering the good coherence with experimental results (*Figure 6*), the model can be used in a structure theory for woven fabrics. The fabric tested *Figure 6* is a plain weave glass fibre fabric. The geometrical parameters and the mechanical coefficients of eqn (1) eq.(2) eq.(3) eq. (4) eq. (5) are the following:

$$L_{0_1} = L_{0_2} = 4.76\text{mm} \quad e_{0_1} = e_{0_2} = 0.238\text{mm} \tag{6}$$

$$A = 0.075\text{mm} \quad B = 0.25\text{N}^{-1} \quad C^1 = C^2 = 38000\text{N} \tag{7}$$

Remarks and limits

The experimental study and the modelling presented in sections "Biaxial test" and "Identification of a biaxial model", are made for plain-weave fabrics. For other geometry of the elementary mesh (twill weave, satin weave,...), phenomena remain of same kind. Some studies, both experimental and of 3D numeric simulation, concerning elementary mesh, are under way in order to show the influence of the geometry in these different cases and to see how the previous model has to be modified.

Angular variations between warp and weft directions during forming is not taken into account in the previous model. Although these distortions are significant, relations between tensions and strains in yarn directions are supposed to be unchanged. This is the conclusion given by the model seen on section "Identification of a biaxial model", when x_1

and $\mathbf{x}_2$ are not orthogonal. Nevertheless, an experimental study, based on a biaxial tensile device that allows to fix a different-from-90 °-angle between the two tensile directions, is being carried out in order to check this assumption.

FINITE ELEMENT SIMULATION

Global equilibrium

An elementary pattern is considered in its initial position (that is to say before deformation) where the two yarn directions are not necessarily perpendicular (see *Figure 9*).

$\boldsymbol{h}_{10}$ and $\boldsymbol{h}_{20}$ are the unit vectors in the warp and weft directions, respectively.

Global equilibrium on the initial configuration is classically written:

$$\int_{\Omega_0} \boldsymbol{S} : D_u(\boldsymbol{E})\eta \mathrm{d}V_0 - \int_{\Omega_0} \boldsymbol{f}_0.\eta \mathrm{d}V_0 + \int_{\Gamma_{t_0}} \boldsymbol{t}_0.\eta \mathrm{d}A_0 = 0 \quad (9)$$

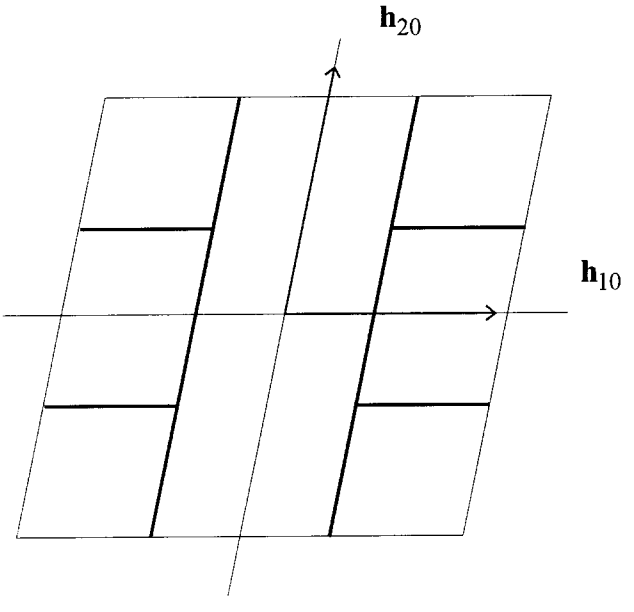

Figure 9 Elementary pattern in its initial position

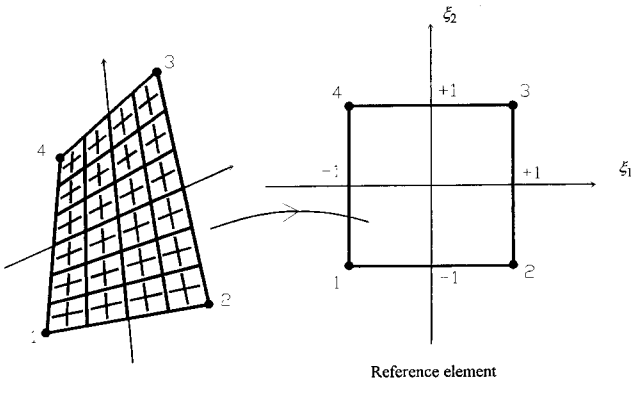

Figure 10 Three dimensional surfacic finite element composed of woven elementary cells

$\forall \eta$ virtual displacement with $\eta = 0$ on Γ_u, part of the frontier with prescribed displacements. $\boldsymbol{f}_0$ are body loads in Ω_0 and $\boldsymbol{t}_0$ are surface loads on Γ_{t_0}, part of the frontier with prescribed efforts. $D_u(\boldsymbol{E})\eta$ is the variation of the Green–Lagrange deformation tensor $\boldsymbol{E}$ (see the nomenclature). Its components in $\boldsymbol{h}^{\alpha 0} \otimes \boldsymbol{h}^{\beta 0}$ are the values measured in the experimental study (see section "Mechanical behaviour of fibre fabrics" and Appendix A).

$\boldsymbol{S}$ is the second Piola–Kirchhoff stress tensor like:

$$\boldsymbol{S}.\boldsymbol{n}_0 = \frac{\mathrm{d}\boldsymbol{f}_0}{\mathrm{d}A_0} \quad (10)$$

where $\mathrm{d}A_0$ is the area, in the initial configuration, of the surfacic element with $\boldsymbol{n}_0$ as its normal, and where $\mathrm{d}\boldsymbol{f}_0$ is the connective transport of the effort on this surface, in the initial configuration. Considering that the yarns have only tensile stiffness (see Appendix B), for a cell directed by $\boldsymbol{h}_{10}$ and $\boldsymbol{h}_{20}$:

$$\boldsymbol{S} = S^{11}\boldsymbol{h}_{10} \otimes \boldsymbol{h}_{10} + S^{22}\boldsymbol{h}_{20} \otimes \boldsymbol{h}_{20} \left(S^{11} \text{ and } S^{22} \geq 0\right) \quad (11)$$

The Lagrangian tensile tensor of second order $\boldsymbol{T}$ is defined by:

$$\boldsymbol{T} = T^{11}\boldsymbol{h}_{10} \otimes \boldsymbol{h}_{10} + T^{22}\boldsymbol{h}_{20} \otimes \boldsymbol{h}_{20} \quad (12)$$

$$\text{with } T^{11} = \int_{A_{10}} S^{11}\mathrm{d}A_0 \quad T^{22} = \int_{A_{20}} S^{22}\mathrm{d}A_0 \quad (13)$$

where A_{10} and A_{20} are the cross sections of yarns directed by $\boldsymbol{h}_{10}$ and $\boldsymbol{h}_{20}$. T^{11} and T^{22} are the moduli of the efforts along warp and weft yarns (see Appendix B).

Notation: all magnitude A, relative to the elementary cell p will be noted ${}^pA$.

Denoting $D_u(\boldsymbol{E})\eta = (D_u(\boldsymbol{E})\eta)_{\alpha\beta}\boldsymbol{h}^{\alpha 0} \otimes \boldsymbol{h}^{\beta 0}$, global Lagrangian equilibrium can be written:

$$\sum_{p=1}^{ncell} \int_{{}^pV_0} {}^pS^{11}\,{}^p\left[D_u(\boldsymbol{E})\eta\right]_{11}\mathrm{d}V_0 + \int_{{}^pV_0} {}^pS^{22}\,{}^p\left[D_u(\boldsymbol{E})\eta\right]_{22}\mathrm{d}V_0 - \int_{\Omega_0} \boldsymbol{f}_0.\eta \mathrm{d}V_0 - \int_{\Gamma_{t_0}} \boldsymbol{t}_0.\eta \mathrm{d}A_0 = 0 \quad (14)$$

$$\forall \eta / \eta = 0 \text{ on } \Gamma_u$$

where ncell is the number of elementary cells of the structure. So:

$$\sum_{p=1}^{ncell} \left[{}^pT^{11}\,{}^p\left(D_u(\boldsymbol{E})\eta\right)_{11}\,{}^p\mathrm{L}_{0_1} + {}^pT^{22}\,{}^p\left(D_u(\boldsymbol{E})\eta\right)_{22}\,{}^p\mathrm{L}_{0_2}\right] - \int_{\Omega_0} \boldsymbol{f}_0.\eta \mathrm{d}V_0 - \int_{\Gamma_{t_0}} \boldsymbol{t}_0.\eta \mathrm{d}A_0 = 0 \quad (15)$$

We note $\mathbf{W}$ the tensor of second order like:

$${}^p\boldsymbol{W} = {}^pT^{11}\,{}^p\mathrm{L}_{0_1}\,{}^p\boldsymbol{h}_{10} \otimes {}^p\boldsymbol{h}_{10} + {}^pT^{22}\,{}^p\mathrm{L}_{0_2}\,{}^p\boldsymbol{h}_{20} \otimes {}^p\boldsymbol{h}_{20} \quad (16)$$

The equilibrium becomes:

$$\sum_{p=1}^{ncell} pD_{\boldsymbol{u}}(E)\eta : {}^{p}\boldsymbol{W} - \int_{\Omega_0} \boldsymbol{f}_0.\boldsymbol{\eta} \mathrm{d}V_0 - \int_{\Gamma_{t_0}} \boldsymbol{t}_0.\boldsymbol{\eta} \mathrm{d}A_0 = 0 \quad \forall \eta/\eta = 0 \text{ on } \Gamma_u \quad (17)$$

Finite elements made of elementary cells

A 3D surfacic finite element is defined. It is made of ncell^e elementary cells, which warp and weft directions are the natural directions of the element (*Figure 10*).

Note: In order to simplify, the presentation is restricted to a four-node element which cells are directed along the natural directions of the element, nevertheless:

—a triangular element is easily built in the same way. It is useful for some initial geometries of the fabric.

—an element which directions are not these of the cell can be obtained in a similar way. In that case, supplementary terms in the matrix components are due to the scalar products between the director-vectors of the yarns and the element. Consequently, the numerical efficiency decreases. For simplicity and numerical efficiency, the element described below is built in the yarn directions. In general, initially flat fabrics can be meshed easily with such elements.

The finite element presented (*Figure 10*) is made of four nodes and uses the classic bilinear interpolation functions:

$$N^1 = \frac{1}{4}(1-\xi_2)(1-\xi_1) \quad N^2 = \frac{1}{4}(1-\xi_2)(1+\xi_1) \quad (18)$$

$$N^3 = \frac{1}{4}(1+\xi_2)(1+\xi_1) \quad N^4 = \frac{1}{4}(1+\xi^2)(1-\xi_1)$$

On each node i, the displacement vector $\boldsymbol{u}^i$ has three components which define the three degrees of freedom per node. The element is isoparametric. If $\boldsymbol{x}_0$ is the initial position of a point, $\boldsymbol{x}$ its current position and $\mathbf{u}$ its displacement:

$$\boldsymbol{x} = \boldsymbol{x}_0 + \boldsymbol{u} \quad \boldsymbol{u} = \sum_{i=1}^{4} N^i \boldsymbol{u}^i \quad \boldsymbol{x}_0 = \sum_{i=1}^{4} N^i \boldsymbol{x}_0^i \quad (19)$$

The classic covariant material vectors are defined from the coordinates ξ_1 and ξ_2 in the reference element:

$$\boldsymbol{g}_{10} = \frac{\partial \boldsymbol{x}_0}{\partial \xi_1} \quad \boldsymbol{g}_1 = \frac{\partial \boldsymbol{x}}{\partial \xi_1} \quad \boldsymbol{g}_{20} = \frac{\partial \boldsymbol{x}_0}{\partial \xi_2} \quad \boldsymbol{g}_2 = \frac{\partial \boldsymbol{x}}{\partial \xi_2} \quad (20)$$

The contravariant frame $(\boldsymbol{g}^{10}, \boldsymbol{g}^{20})$ is associated to the covariant frame $(\boldsymbol{g}_{10}, \boldsymbol{g}_{20})$ by:

$\boldsymbol{g}^{\alpha 0}.\boldsymbol{g}_{\beta 0} = \delta_\beta^\alpha$ (Kronecker delta) α and β are indexes equal to 1 or 2 (21)

The components of the Green–Lagrange strain tensor in the contravariant frame

$$\boldsymbol{E} = \bar{E}_{\alpha\beta} \boldsymbol{g}^{\alpha 0} \otimes \boldsymbol{g}^{\beta 0} \quad (22)$$

are classically linked to the displacements:

$$\bar{E}_{\alpha\beta} = \frac{1}{2}\left(\frac{\partial \boldsymbol{u}}{\partial \xi_\alpha}.\boldsymbol{g}_{\beta 0} + \frac{\partial \boldsymbol{u}}{\partial \xi_\beta}.\boldsymbol{g}_{\alpha 0} + \frac{\partial \boldsymbol{u}}{\partial \xi_\alpha}.\frac{\partial \boldsymbol{u}}{\partial \xi_\beta} \right) \quad (23)$$

They define the terms of the strain interpolation matrix:

$$D_{\boldsymbol{u}}(\bar{E}_{\alpha\beta})\eta = \bar{B}_{\alpha\beta s}\eta_s \quad (24)$$

$$\text{with } \bar{B}_{\alpha\beta s} = \frac{1}{2}\left[\frac{\partial N^k}{\partial \xi_\alpha}(g_{\beta 0})_m + \frac{\partial N^k}{\partial \xi_\beta}(g_{\alpha 0})_m + \left(\frac{\partial N^k}{\partial \xi_\alpha}\frac{\partial N^q}{\partial \xi_\beta} + \frac{\partial N^q}{\partial \xi_\alpha}\frac{\partial N^k}{\partial \xi_\beta} \right)(u^q)_m \right] \quad (25)$$

and

$$k = int\left(\frac{s+2}{3}\right) \quad m = s - 3(k-1) \quad q \in [1,4]$$

Newton method

The equilibrium eqn (17), associated with the finite element discretization:

$$G(\boldsymbol{u},\eta) = \sum_{elt} \sum_{p=1}^{ncell^e} {}^{p}D_{\boldsymbol{u}}(\boldsymbol{E})\eta : {}^{p}\boldsymbol{W} - \int_{\Omega_0^e} \boldsymbol{f}_0 \eta \mathrm{d}V_0 - \int_{\Gamma_{t_0}^e} \boldsymbol{t}_0.\boldsymbol{\eta} \mathrm{d}A_0 = 0 \ \forall \eta/\eta = 0 \text{ on } \Gamma_u \quad (26)$$

is a non-linear equation, considering the geometric non-linearities and the non-linear behaviour that links up the tensions and the strains, like defined in section "Mechanical behaviour of fibre fabrics". This equation is solved by a Newton-type scheme for each increment.

$G(\mathbf{u},\eta) = 0 \ \forall \eta/\eta = 0$ on Γ_u is replaced by a series of iterations j where

$$D_{\boldsymbol{u}^j} G(\boldsymbol{u},\eta)\Delta \boldsymbol{u}^j = -G(\boldsymbol{u}^j,\eta) \quad (28)$$

And then:

$$\underbrace{\sum_{elt} \sum_{p=1}^{ncell^e} D_{\boldsymbol{u}^j}\left({}^{p}D_{\boldsymbol{u}}(\boldsymbol{E})\eta\right)\Delta \boldsymbol{u}^j : {}^{p}\boldsymbol{W}\left({}^{p}\boldsymbol{E}^j\right)}_{(a)^j} + \underbrace{\sum_{ell} \sum_{p=1}^{ncell^e} {}^{p}D_{\boldsymbol{u}^j}(\boldsymbol{E})\eta : {}^{p}\left[\frac{\partial \boldsymbol{W}(\boldsymbol{E})}{\partial \boldsymbol{E}}\right]^j : {}^{p}D_{\boldsymbol{u}^j}(\boldsymbol{E})\Delta \boldsymbol{u}^j}_{(b)^j} \quad (29)$$

$$= \underbrace{-\sum_{elt} \sum_{p=1}^{ncell^e} \left({}^{p}D_{\boldsymbol{u}^j}(\boldsymbol{E})\eta\right)^j : {}^{p}\boldsymbol{W}\left({}^{p}\boldsymbol{E}^j\right)}_{(c)^j} + \int_{\Omega_0^e} \boldsymbol{f}_0.\boldsymbol{\eta} \mathrm{d}V_0 + \int_{\Gamma_{t_0}^e} \boldsymbol{t}_0.\boldsymbol{\eta} \mathrm{d}A_0$$

$$\forall \eta/\eta = 0 \text{ on } \Gamma_u$$

Taking into account the nodal interpolation (19), this

expression can be written as:

$$\sum_{elt} \eta^{e\,T}\left(\boldsymbol{K}^e + \boldsymbol{K}_\sigma^e\right)^j \left(\Delta \boldsymbol{u}^e\right)^j = \sum_{elt} \eta^{e\,T}\left(\boldsymbol{F}_{ext}^e - \left(\boldsymbol{F}_{int}^e\right)^j\right) \quad (30)$$

where η^e and $(\Delta u^e)^j$ are the nodal elementary component vector of the virtual displacement and of the displacement increment, respectively. $(\boldsymbol{K}^e)^j$ is the elementary stiffness matrix at iteration j; $(\boldsymbol{K}_\sigma^e)^j$ is the elementary geometrical stiffness matrix at iteration j; $(\boldsymbol{F}_{int}^e)^j$ is the elementary interior load vector at iteration j; $\boldsymbol{F}_{ext}^e$ is the elementary load vector.

Since eqn (28) eq. (29) eq. (30) hold for kinematically admissible to zero virtual displacement, eqn (30) gives the displacement increment at iteration j as the solution of the incremental linear system

$$\left(\boldsymbol{K} + \boldsymbol{K}_\sigma\right)^j \left(\Delta \boldsymbol{u}\right)^j = \boldsymbol{F}_{ext} - \left(\boldsymbol{F}_{int}\right)^j \quad (31)$$

with, if A_{elt} is the assemblage operator on all the elements of the structure,

$$\boldsymbol{K}^j = \underset{elt}{A}\left(\boldsymbol{K}^e\right)^j \quad \left(\boldsymbol{K}_\sigma\right)^j = \underset{elt}{A}\left(\boldsymbol{K}_\sigma^e\right)^j \quad \left(\boldsymbol{F}_{int}\right)^j = \underset{elt}{A}\left(\boldsymbol{F}_{int}^e\right)^j \quad (32)$$

In the following section, the calculation of the elementary matrices is detailed for a four-node finite element made of fibres.

Calculation of stiffness and internal load matrices

Afterwards, indexes p (number of the cell) and j (number of the iteration) will be omitted, for simplicity reasons.

Internal load vector. The elementary internal load vector is given by part (c) of (29).

$$(c) = \sum_{p=1}^{ncell^e} \left(D_u(\boldsymbol{E})\eta\right) : \boldsymbol{W}(\boldsymbol{E}) = \left(\eta^e\right)^T \boldsymbol{F}_{int}^e = \eta_s^e \left(F_{int}^e\right)_s \quad (33)$$

$$= \sum_{p=1}^{ncell^e} \bar{B}_{\alpha\beta s}\eta_s \left[\mathrm{L}_{0_1} T^{11}\left(\boldsymbol{g}^{\alpha 0} \otimes \boldsymbol{g}^{\beta 0}\right) : \left(\boldsymbol{h}_{10} \otimes \boldsymbol{h}_{10}\right) + \mathrm{L}_{o_2} T^{22}\left(\boldsymbol{g}^{\alpha 0} \otimes \boldsymbol{g}^{\eta 0}\right) : \left(\boldsymbol{h}_{20} \otimes \boldsymbol{h}_{20}\right)\right] \quad (34)$$

$$\text{So}: \left(F_{int}^e\right)_s = \sum_{p=1}^{ncell^e} \bar{B}_{11s}\mathrm{L}_{0_1} T^{11} \frac{1}{\|\boldsymbol{g}_{10}\|^2} + \bar{B}_{22s}\mathrm{L}_{0_2} T^{22} \frac{1}{\|\boldsymbol{g}_{20}\|^2} \quad (35)$$

Geometrical stiffness matrix. The expression of the geometrical stiffness matrix is given by part (a) of (29).

$$(a) = \sum_{p=1}^{ncell^e} D_u\left(D_u\left(\bar{E}_{\alpha\beta}\right)\eta\right)\Delta \boldsymbol{u}\bar{W}^{\alpha\beta} = \eta^{e^T} \boldsymbol{K}_\sigma^e \Delta \boldsymbol{u}^e = \left(\eta^e\right)_r \left(K_\sigma^e\right)_{rs} \left(\Delta u^e\right)_s \quad (36)$$

where $\bar{W}^{\alpha\beta}$ are the components of $\mathbf{W}$ in the frame $\boldsymbol{g}_{\alpha 0} \otimes \boldsymbol{g}_{\beta 0}$

$$\boldsymbol{W} = T^{\alpha\alpha}\mathrm{L}_{0_\alpha} \boldsymbol{h}_{\alpha 0} \otimes \boldsymbol{h}_{\alpha 0} = \bar{W}^{\alpha\beta} \boldsymbol{g}_{\alpha 0} \otimes \boldsymbol{g}_{\beta 0} \quad (37)$$

$$\text{So}: \bar{W}^{11} = \mathrm{L}_{0_1} T^{11} \frac{1}{\|\boldsymbol{g}_{10}\|^2} \bar{W}^{22} = \mathrm{L}_{0_2} T^{22} \frac{1}{\|\boldsymbol{g}_{20}\|^2} \bar{W}^{12} = \bar{W}^{21} = 0 \quad (38)$$

Differentiation of eqn (23) gives:

$$D_u\left(D_u\left(\bar{E}_{\alpha\beta}\right)\eta\right)\Delta \boldsymbol{u} = \frac{1}{2}\left(\frac{\partial \eta}{\partial \xi_\alpha} \cdot \frac{\partial \Delta \boldsymbol{u}}{\partial \xi_\beta} + \frac{\partial \eta}{\partial \xi_\beta} \cdot \frac{\partial \Delta \boldsymbol{u}}{\partial \xi_\alpha}\right) \quad (39)$$

$$\text{so that}: (a) = \sum_{p=1}^{ncell^e} \left(\frac{\partial \eta}{\partial \xi_\alpha} \cdot \frac{\partial \Delta \boldsymbol{u}}{\partial \xi_\alpha}\right) \bar{W}^{\alpha\alpha}$$

Considering the nodal interpolation of the displacements:

$$(a) = \sum_{p=1}^{ncell^e} \bar{W}^{\alpha\alpha} \frac{\partial N^k}{\partial \xi_\alpha} \frac{\partial N^q}{\partial \xi_\alpha} \left(\eta^k\right)_m \left(\Delta u^q\right)_m = \left(\eta^e\right)_r \left(K_\sigma^e\right)_{rs} \left(\Delta u^e\right)_s \quad (40)$$

with k,q ϵ[1,n nodes = 4] and mϵ[1, n components = 3]

Denoting k = int $\left(\frac{r+2}{3}\right)$ and q = int $\left(\frac{s+2}{3}\right)$

If $r - 3k = s - 3q$

$$\left(K_\sigma^e\right)_{rs} = \sum_{p=1}^{ncell^2} \mathrm{L}_{0_1} T^{11} \frac{1}{\|\boldsymbol{g}_{10}\|^2} \frac{\partial N^k}{\partial \xi_1} \frac{\partial N^q}{\partial \xi_1} + \mathrm{L}_{0_2} T^{22} \frac{1}{\|\boldsymbol{g}_{20}\|^2} \frac{\partial N^k}{\partial \xi_2} \frac{\partial N^q}{\partial \xi_2} \quad (41)$$

$$\text{If } r - 3k \neq s - 3q \quad \left(K_\sigma^e\right)_{rs} = 0 \quad (42)$$

Stiffness matrix. The stiffness matrix is obtained from part (b) of (29):

$$(b) = \sum_{p=1}^{ncell^e} D_u(\boldsymbol{E})\eta : \frac{\partial \boldsymbol{W}(\boldsymbol{E})}{\partial \boldsymbol{E}} : D_u(\boldsymbol{E})\Delta \boldsymbol{u} = \eta^{e^T} \boldsymbol{K}^e \Delta \boldsymbol{u}^e = \left(\eta^e\right)_r \left(K^e\right)_{rs} \left(\Delta u^e\right)_s \quad (43)$$

$\boldsymbol{D} = \dfrac{\partial \boldsymbol{W}}{\partial \boldsymbol{E}}$ is a behaviour tensor of the fourth order.

$$\boldsymbol{D} = \frac{\partial \boldsymbol{W}}{\partial \boldsymbol{E}} = \bar{D}^{\alpha\beta\gamma\delta} \boldsymbol{g}_{\alpha 0} \otimes \boldsymbol{g}_{\beta 0} \otimes \boldsymbol{g}_{\gamma 0} \otimes \boldsymbol{g}_{\delta 0} = \mathrm{L}_{0_\alpha} \frac{\partial T^{\alpha\alpha}}{\partial E_{\beta\beta}} \boldsymbol{h}_{\alpha 0} \otimes \boldsymbol{h}_{\alpha 0} \otimes \boldsymbol{h}_{\beta 0} \otimes \boldsymbol{h}_{\beta 0} \quad (44)$$

Terms $\dfrac{\partial T^{\alpha\alpha}}{\partial E_{\beta\beta}}$ are known from the behaviour modelling done in section "Mechanical behaviour of fibre fabrics".

$$\text{So that}: \bar{D}^{1111} = \frac{\mathrm{L}_{0_1}}{\|\boldsymbol{g}_{10}\|^4} \frac{\partial T^{11}}{\partial E_{11}} \quad \bar{D}^{2222} = \frac{\mathrm{L}_{0_2}}{\|\boldsymbol{g}_{20}\|^4} \frac{\partial T^{22}}{\partial E_{22}}$$

and

$$\bar{D}^{1122} = \frac{1}{\|\boldsymbol{g}_{10}\|^2 \|\boldsymbol{g}_{20}\|^2} \left(\frac{\partial T^{11}}{\partial E_{22}}\right) \bar{D}^{2211} = \frac{1}{\|\boldsymbol{g}_{10}\|^2 \|\boldsymbol{g}_{20}\|^2} \left(\frac{\partial T^{22}}{\partial E_{11}}\right) \quad (45)$$

Other terms $\bar{D}^{\alpha\beta\gamma\delta}$ are zero.

The strain interpolation (24) gives:

$$(b) = \sum_{p=1}^{ncell} \bar{B}_{\alpha\beta r}(\eta^e)_r \bar{D}^{\alpha\beta\gamma\delta} \bar{B}_{\gamma\delta s}(\Delta u^e)_s = (\eta^e)_r (K^e)_{rs} (\Delta u^e)_s \tag{46}$$

$$\text{then : } (K^e)_{rs} = \sum_{p=1}^{ncell} \bar{B}_{\alpha\beta r} \bar{D}^{\alpha\beta\gamma\delta} \bar{B}_{\gamma\delta s} \tag{47}$$

The knowledge of the behaviour that links the tensions T^{11}, T^{22} with the strains E_{11}, E_{22}, as defined in section "Mechanical behaviour of fibre fabrics", then allows the

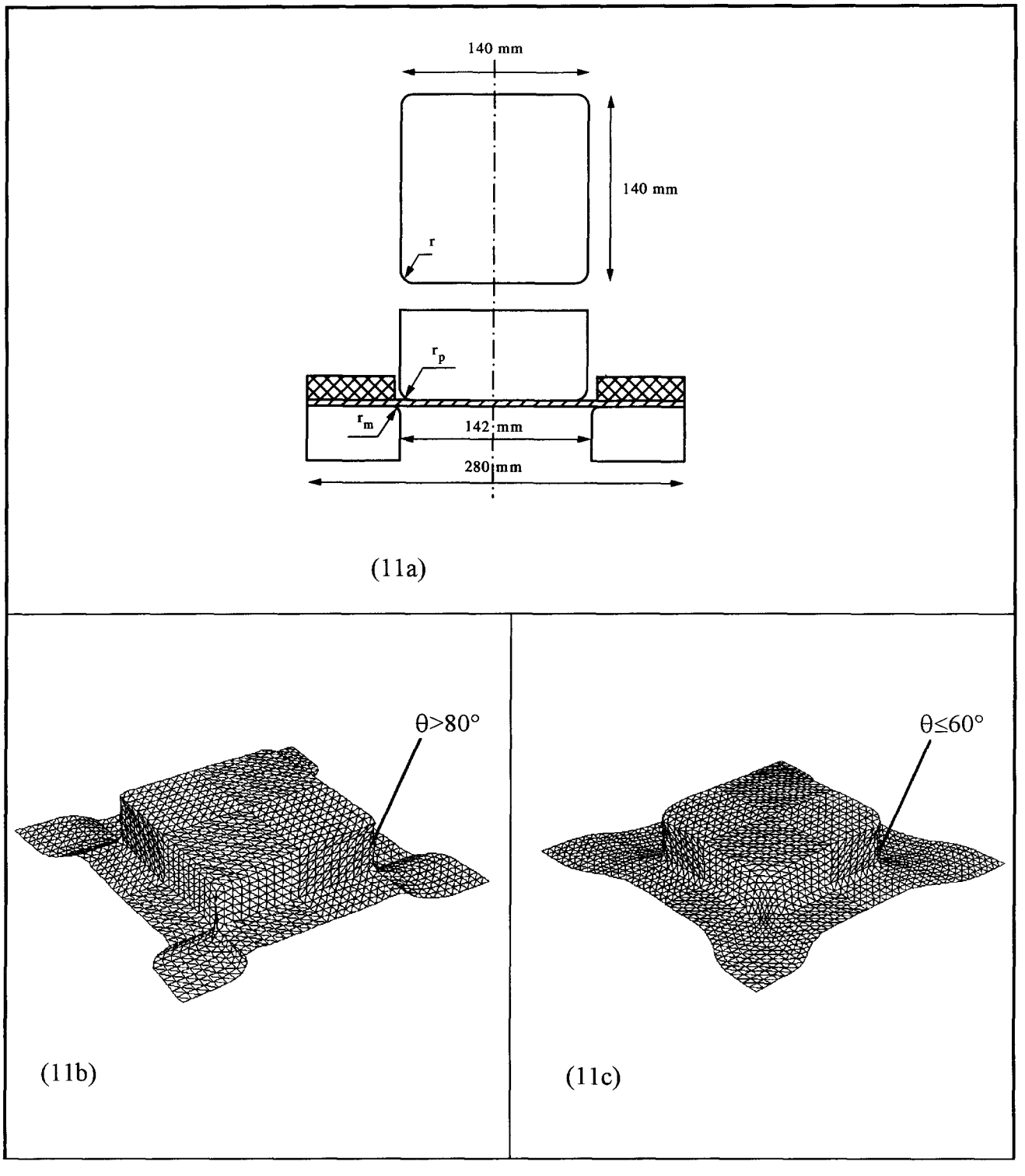

Figure 11 Simulation of shaping with a square punch and die. Definition of the possible geometry of the tools. (a) Geometry of the tools. (b) Final computed shape of the fabric for $r = 5$ mm; $r_p = 6$ mm; $r_m = 5$ mm. (c) Final computed shape of the fabric for $r = 10$ mm; $r_p = 15$ mm; $r_m = 10$ mm

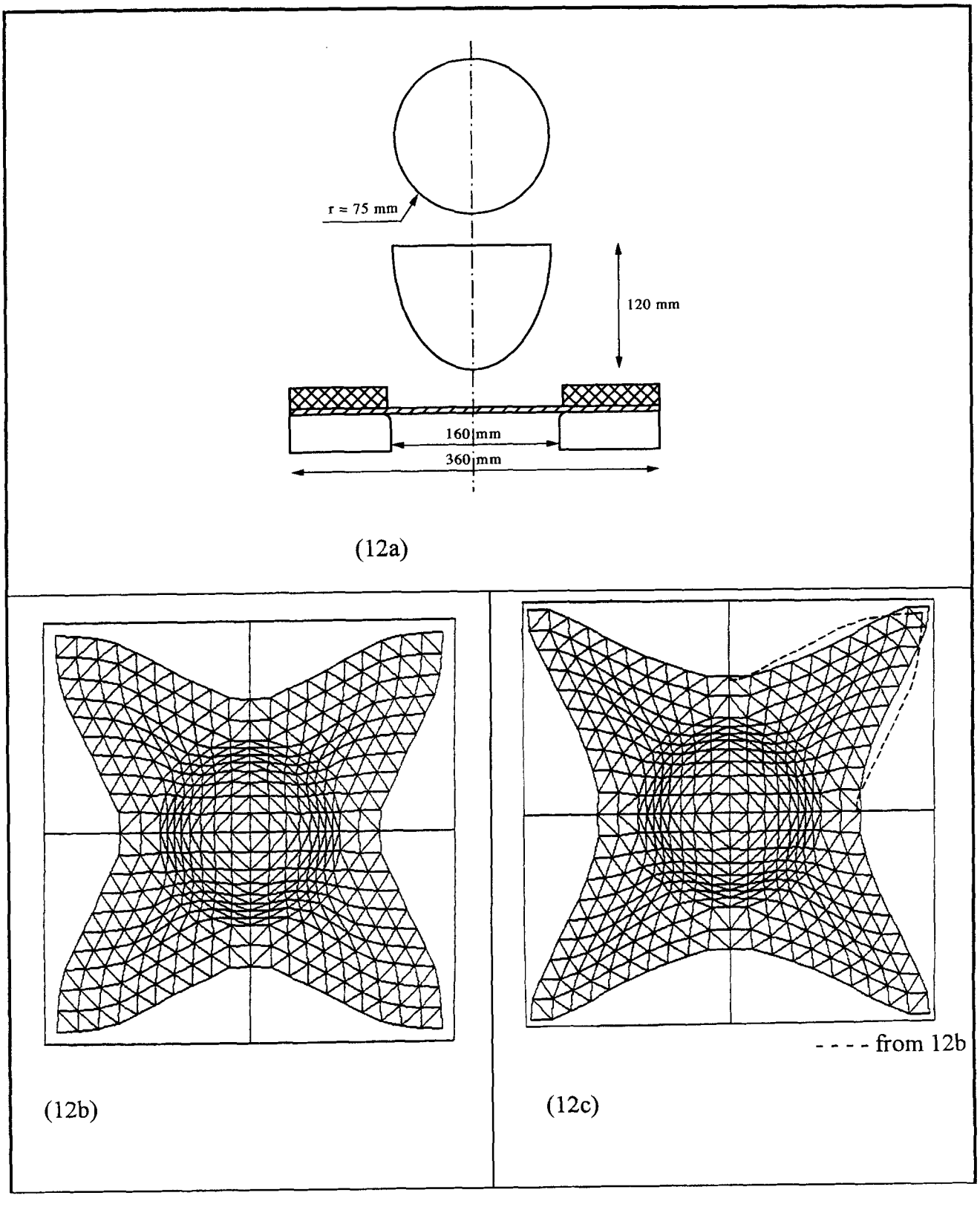

Figure 12 Simulation of shaping with ellipsoidal punch and die. Influence of undulations. (a) Geometry of the tools. (b) Final computed shape of the fabric without accounting for undulation variations. (c) Final computed shape of the fabric accounting for undulation variations

calculation of elementary stiffness matrices (47), (41) and of the internal load vector (35).

Remark 1: The expressions given by (35), (41) and (47) are explicit. They give directly the values of the matrix terms without any matrix multiplication or intermediary integration. It results from it a great numeric efficiency of the formulation.

Remark 2: In order that the behaviour defined in section

"Mechanical behaviour of fibre fabrics" could be used in the previous matrix expressions, it is necessary:

—either to make the assumption that the strains in the yarn direction are low enough to make $E_{\alpha\alpha}$ similar to $\epsilon_{\alpha\alpha}$. It is the case for the fabrics tested in this paper, which strains at breaking point are lower than 2%;
—or to modify the behaviour expressions in order to link T^{11}, T^{22} to E_{11},E_{22}.

NUMERICAL EXAMPLES

Drawing with a square punch and die

An initially square blank made of a glass fibre fabric is shaped into a square box[20] (*Figure 11*a). This operation is the first stage of a R.T.M. manufacturing process. A pressure equal to 1 MPa is applied on the blank holder, and the friction coefficient between the fabric and the tool is set to 0.2. The geometry of the final square box is far from being developable. The shape is obtained by deformation of the fabric due to large angular variations of the warp and weft directions, especially near the corners of the box. The feasibility of the shaping operation is restricted by the limitation of these angular variations. For the usual glass fibre fabrics used in the R.T.M. process[18] the maximum value of these angular variations are close to 60°. Results of simulations of the shaping operation are shown *Figure 11*b and c for two sets of radius for the punch and the die. These radii mainly influence the maximum values of the angular variations of the yarn directions. The first geometry of the tools ($r = 5$ mm; $r_p = 6$ mm; $r_m = 5$ mm) leads to angular variations (*Figure 11*b) greater than 80°; these values are impossible for the fabric. On the opposite, the second geometry proposed for the tools ($r = 10$ mm; $r_p = 15$ mm; $r_m = 10$ mm) leads to angular variations smaller than 60° and the shaping operation appears to be possible.

This example shows one of the main interest of the simulation tool that allows to verify the feasibility of a drawing operation for a given geometry of the tool and a given fabric, before the manufacturing of the punch and die. An other main aspect is the knowledge of the tensions in the yarns which can be high if a significant load is applied on the blank holder. In this first example, the behaviour of the fabric is supposed to be only dependent on the yarn tensile behaviour. This assumption is restricted to fabrics with a very flat geometry of the weaving. Other examples based on this assumption can be found in references [19], [20] and [21].

Drawing with an ellipsoidal punch. Influence of the undulation variations

An initially square blank made of a glass fibre fabric is shaped by an ellipsoidal punch (*Figure 12*a). The computation is first made (*Figure 12*b) neglecting the influence of the undulations and interactions on the fabric behaviour, i.e. considering that the tensile behaviour of a yarn is only depending on its own tensile strain as shown in *Figure 8*. *Figure 12*c presents the deformed shape obtained when the influence of the yarn undulation variations are taken into account. The constitutive law given by eqn (1) eq. (2) eq. (3) eq. (4) eq. (5) is used for the fabric behaviour. The coefficients given in eq. (6) and eq. (7) are these of the plain weave glass fibre fabric tested in *Figure 6*. The difference between the two computed shape is shown in *Figure 12*c. It is not very large because the fabric under consideration is rather flat.

SUMMARY AND CONCLUSIONS

The proposed simulation tool allows to test the feasibility of the drawing of a given fabric into a given 3D shape. The example of the shaping of a square box shows that a geometry can be accepted or not from the computed strains in the fabric. The values of the tensions in the yarns can also be checked during the shaping. The simulation is based on finite elements made of woven fabric where the deformation energy is obtained from those of each elementary woven cell. The behaviour liking up the tension state and the stress state includes the effect of the undulation variations of the yarns when the fabric is deformed. The proposed behaviour model has been identified and validated from biaxial tensile tests. The influence of undulation variations in a shaping process simulation has been shown. It is not very important in the presented example because the fabric under consideration is rather flat and because the deformations involved by the shaping are large in comparison with the domain of influence of the undulation variations. Other cases are now on study, especially shaping simulations using different fabrics. The proposed approach is also applied to the simulation of the mechanical deformations of boat sails.[22] In that case, the deformation of the fabric is lower and the influence of the undulation variations is more important.

REFERENCES

1. Reyne, M., *Technologie des composites*, (Eds Hermes), Paris, 1990.
2. Gay, D., *Matériaux composites* (Eds Hermes), Paris, 1987.
3. Blanlot, R., Billoet, J.-L. and Gachon, H., Study of non polymerised prepreg fabrics in "off-axes" tests. In *Proceedings of ICCM/9*. Madrid, 1993, pp. 576–583.
4. Schweizerhof, K., Weimar, K., Hallquist, J.O. and Stillman, W., Improving standard shell elements, friction models and contact algorithms for the efficient solution of sheet metal forming problems with LS-DYNA3D, *Proceedings of "F.E. Simulation of 3D sheet metal forming processes in automotive industry"*, VDI 894, 1991, pp. 499–516.
5. Onate, E. and Agelet de Saracibar, C., Numerical modeling of sheet metal forming problems. In *Numerical Modelling of Material Deformation Processes*, Hartley, P.; Pillinger I. and Sturgess C., Ed., Springer-Verlag, 1992, pp. 318–357.
6. Boubakar, M.L., Boisse, P. and Gelin, J.C., Numerical implementation of orthotropic plasticity for sheet metal forming analysis, In *J. of Material Processing Technology*, 1997 (To appear).
7. Bergsma, O.K. and Huisman, J., Deep drawing of fabric reinforced thermoplastics. In *Proceedings of the 2nd Int. Conf. on Computer Aided Design in Composite Material Technology*, Ed. by CA Brabbia and all, Springer Verlag, 1988, pp. 323–333.

8. Van De Ween, F., Algorithms for draping fabrics on doubly curved surfaces. *Int. J. Num. Meth. Engng.*, 1991, **31**, 1415–1426.
9. Ishikawa, T. and Chout, T., Non-linear behaviour of woven fabric composites. *J. of composites materials*, 1983, **17**, 399–413.
10. Lene, F., Technique d'homogénéisation des composites à renforts tissés. *Mécanique Matériaux Electricité*, 1990, **433**, 24–28.
11. Glaessgen, E.H., Pastore, C.M., Griffin, O.H. and Birger, A., Geometrical and finite element modelling of textile composites. *Composites Part B*, 1996, **27B**, 43–50.
12. Ferron, G., *Dispositif de traction biaxiale*, Document Techmetal, Mezieres-Les-Metz, 1992.
13. Borr, M. and Boisse, P., Détermination du comportement biaxial des tissus de fibres de verre. Mesure optique de la déformation, In *Proceedings of Photomécanique 95*, Cachan, France, 1995, pp. 187–194.
14. Kawabata, S., Non-linear mechanics of woven and knitted materials (Eds Elsevier). *Textile structure composites*, 1989, **3**, 67–116.
15. Borr, M., Comportement et modélisation numérique des structures tissées, PhD thesis, University of Franche-Comté, 1997 (to appear).
16. Kawabatta, S., Masako, N. and Kawai, H., The finite deformation theory of plain weave fabrics, Part I, Part II, Part III . *J. of the Textile Institute*, 1973, **64**, 21–83.
17. Realf, M.L., Boyce, M.C. and Backer, S., A micromechanical approach to modelling tensile behaviour of woven fabrics, In *Use of plastic and plastic composites: material and mechanic issue*, Stokes, V.J., Ed., ASME, New-York, **46**, 1993, pp. 285–293.
18. Boisse, P., Gelin, J.-C. and Sabhi, H., Experimental study and finite element simulation of a glass fibre fabric shaping process, In *Use of plastic and plastic composites: material and mechanics issue*, Stokes, V.J., Ed., ASME, New-York, **46**, 1993, pp. 587–608.
19. Boisse, P., Cherouat, A., Gelin, J.-C. and Sabhi, H., Manufacturing of thin composite structures by the R.T.M. process. Numerical simulation of the shaping operation, In *Proceedings of the 9th national conference on composites*, AMAC, Saint-Etienne, France, 1994, pp. 95–104.
20. Cherouat, A., Modélisation numérique par la méthode des éléments finis du préformage des tissus de fibres de verre, PhD thesis, University of Franche-Comté, 1994.
21. Boisse, P., Cherouat, A., Gelin, J.-C. and Sabhi, H., Experimental study and finite element simulation of a glass fibre fabric shaping process. *Polymer composites*, 1995, **16**, 83–95.
22. Valette, J., Module de calcul éléments finis pour la simulation des voiles de bateaux, Internal report, CRAIN, La Rochelle, France, 1996.

APPENDIX

A. Components of the Green–Lagrange strain tensor in $\boldsymbol{h}^{\alpha 0} \otimes \boldsymbol{h}^{\beta 0}$

$$\text{Let } \boldsymbol{E} = E_{\alpha\beta}\boldsymbol{h}^{\alpha 0} \otimes \boldsymbol{h}^{\beta 0} \tag{A1}$$

where vectors $\boldsymbol{h}^{\alpha 0}$ define the contravariant base, associated to $\boldsymbol{h}_{\alpha 0}$, i.e.

$$\boldsymbol{h}_{\alpha 0}.\boldsymbol{h}^{\beta 0} = \delta_\alpha^\beta \tag{A2}$$

($\boldsymbol{h}^{10}$,$\boldsymbol{h}^{20}$ are in the plane defined by $\boldsymbol{h}_{10}$,$\boldsymbol{h}_{20}$)
Considering an initial elementary vector $\mathrm{d}\boldsymbol{x}_0$ which is $\mathrm{d}\boldsymbol{x}$ after deformation, $\boldsymbol{E}$ is defined by:

$$\mathrm{d}\boldsymbol{x}.\mathrm{d}\boldsymbol{x} - \mathrm{d}\boldsymbol{x}_0.\mathrm{d}\boldsymbol{x}_0 = 2\mathrm{d}\boldsymbol{x}_0.\boldsymbol{E}.\mathrm{d}\boldsymbol{x}_0 \tag{A3}$$

Let an initial elementary vector be directed by $\boldsymbol{h}_{10}$: $\mathrm{d}\boldsymbol{x}_0$

$$= \mathrm{d}l_0\boldsymbol{h}_{10} \tag{A4}$$

It is changed into $\mathrm{d}\boldsymbol{x} = \mathrm{d}l\boldsymbol{h}_1$.

$$\text{(A3) gives : } \frac{\mathrm{d}l^2 - \mathrm{d}l_0^2}{2\mathrm{d}l_0^2} = \boldsymbol{h}_{10}.\boldsymbol{E}.\boldsymbol{h}_{10}$$

$$= \boldsymbol{h}_{10}.\left(E_{\alpha\beta}\boldsymbol{h}^{\alpha 0} \otimes \boldsymbol{h}^{\beta 0}\right).\boldsymbol{h}_{10} = E_{11}$$

Therefore, E_{11} is the measured strain along the material direction, initially directed by $\boldsymbol{h}_{10}$.

B. Second Piola Kirchhoff tensor and Lagrangian tensile tensor for fabrics

We are considering a section of the elementary cell, containing $\boldsymbol{h}_{20}$ and therefore its normal $\boldsymbol{n}_0 = \dfrac{\boldsymbol{h}^{10}}{\|\boldsymbol{h}^{10}\|}$. Its cross section is noted $\mathrm{A'}_{10}$.

$$\text{Considering(10) : } \int_{\mathrm{A'}_{10}} \boldsymbol{S}.\frac{\boldsymbol{h}^{10}}{\|\boldsymbol{h}^{10}\|}\mathrm{d}A_0 = T^{10}\boldsymbol{h}_{10} \tag{B1}$$

$T^{10}\,\mathbf{h}_{10}$ is the load on the cell, along the yarn directed by $\boldsymbol{h}_{10}$.
In particular, $S^{\alpha\beta}$ are the components of $\boldsymbol{S}$ in $\boldsymbol{h}_{\alpha 0} \otimes \boldsymbol{h}_{\beta 0}$:

$$\boldsymbol{S} = S^{11}\boldsymbol{h}_{10} \otimes \boldsymbol{h}_{10} + S^{22}\boldsymbol{h}_{20} \otimes \boldsymbol{h}_{20} + S^{12}\boldsymbol{h}_{10} \otimes \boldsymbol{h}_{20} + S^{21}\boldsymbol{h}_{20} \otimes \boldsymbol{h}_{10} \tag{B2}$$

Then:

$$\boldsymbol{S}.\boldsymbol{h}_{10} = S^{11}\boldsymbol{h}_{10}\left(\boldsymbol{h}_{10}.\boldsymbol{h}^{10}\right) + S^{22}\boldsymbol{h}_{20}\left(\boldsymbol{h}_{20}.\boldsymbol{h}^{10}\right) + S^{12}\boldsymbol{h}_{10}\left(\boldsymbol{h}_{20}.\boldsymbol{h}^{10}\right) + S^{21}\boldsymbol{h}_{20}\left(\boldsymbol{h}_{10}.\boldsymbol{h}^{10}\right) \tag{B3}$$

So:

$$\boldsymbol{S}.\boldsymbol{h}_{10} = S^{11}\boldsymbol{h}_{10} + S^{21}\boldsymbol{h}_{20} \tag{B4}$$

Therefore:

$$S^{21} = 0 \tag{B5}$$

and

$$\frac{1}{\|\boldsymbol{h}^{10}\|}\int_{\mathrm{A'}_{10}} S^{11}\mathrm{d}A_0 = T^{10} = \int_{\mathrm{A}_{10}} S^{11}dA_0 \tag{B6}$$

Consequently, and if doing the same calculation in the other yarn direction, $\boldsymbol{S}$ is in the form used in (11).

$$\boldsymbol{S} = S^{11}\boldsymbol{h}_{10} \otimes \boldsymbol{h}_{10} + S^{22}\boldsymbol{h}_{20} \otimes \boldsymbol{h}_{20} \quad \left(S^{11} \text{ and } S^{22} \geq 0\right) \tag{B7}$$

and the component of the tensile tensor $T^{\alpha\alpha} = \int_{\mathrm{A}_{10}} S^{\alpha\alpha}\mathrm{d}A_0$ is equal to $T^{\alpha 0}$, modulus of the effort along $\boldsymbol{h}_{\alpha 0}$, which can be measured during the experimental study.